Insight into the Evolution of the Cellulose Microstructure Through the Enzyme Pretreatment Method

Qijun Ding
Qilu University of Technology
Limin Jing
Qilu University of Technology
Wenjia Han
Qilu University of Technology
Yanpeng Guan
Qilu University of Technology
Yifei Jiang
Qilu University of Technology
Peng Du
Qilu University of Technology
Chaojun Wu
Qilu University of Technology
Ronggang Li (lrg923@163.com)
Qilu University of Technology
Xia Li
Qilu University of Technology

Research Article

Keywords: cellulosic fiber, enzymatic pretreatment, hydrogen bond, Fourier transform infrared spectroscopy, two-dimensional correlation spectroscopy

Posted Date: April 26th, 2021

DOI: https://doi.org/10.21203/rs.3.rs-391422/v1

Abstract

In this work, the changes of properties and microstructure of cellulose (bleached hardwood kraft pulp (BHKP)) subjected to different enzyme pretreatment times (0–10 h) were explored for further fibrillation. The various properties of the pretreated cellulose gradually decrease with the elapse of time relative to the pristine material, such as yield, water retention value, aspect ratio and degree of polymerization, etc. Enzyme pretreatment can promote the peeling of fibrils and loosen the amorphous areas of cellulose identified by Scanning Electron Microscope (SEM) and X-ray diffraction (XRD). A thorough investigation of the relation between pretreatment and evolution of inter-/intra-molecular H-bonds in cellulose was conducted including content and cleave sequence of H-bonds by Fourier transform infrared spectroscopy (FTIR), second derivative analysis and generalized two-dimensional correlation spectroscopy (2DCOS). The intermolecular H-bonds with the most significant decrease in content was cleaved first relative to the intramolecular H-bonds. These discoveries provide theoretical support to more effective pretreatment method for commercial production of fibrils from cellulosic fibers.

1. Introduction

In recent years much more attention has been paid to nanoscaled bio-based material for various application. Numerous renewable and biodegradable bio-based fiber composite materials have been developed to obtain the next generation of sustainable and green materials in this application field (Jonoobi et al. 2015; Zhu et al. 2016). Cellulose is the most abundant renewable natural biopolymer and regaining importance as a renewable chemical resource to replace petroleum-based materials. In addition to biodegradability and renewability, the production of cellulose nanofibrils (CNFs) have added promising properties such as high mechanical properties, high specific surface area and high transparency, which are widely used in the fields of food, cosmetic, pharmaceutical, flexible displays and papermaking (Zhu et al. 2016). However, one of the bottlenecks in commercial production of CNF is the high energy consumption in the mechanical refining process of CNF production.

Cellulose is a linear homopolysaccharide composed of β-1, 4-linked D-glucopyranose units with a high degree of polymerization (DP). The three hydroxyl groups of the monomer and their ability to form hydrogen bonds play an important role in leading the crystalline packing, which provide cellulose with a stable crystal structure and high crystallinity (Dufresne and Alain 2017; Zhu et al. 2016). Therefore, energy consumption is the main drawback for mechanical approaches to diminish cellulosic fibers into nanofibrils (Daud et al. 2015). And CNF defibrillation requires intensive mechanical treatment and less energy utilization will result in less cellulose fibrils and less nanofiber production (Nechyporchuk et al. 2016). To overcome this shortcoming, researchers had basically proposed three different strategies for pretreatment of cellulose fibers before mechanical treatment: (1) limit the hydrogen bonding in the system, and (2) add repulsive charges, and (3) reduce the DP or amorphous connection between individual filaments (Lavoine et al. 2012). It is worth noting that the proper pretreatment of cellulose fibers can promote the accessibility of hydroxyl groups, increase the inner surface, change the crystallinity and cleave the cellulose hydrogen bonds, improve the reactivity of the fibers and effectively

reduce the energy consumption during the fibrillation process, such as alkaline-acid, enzymatic hydrolysis, TEMPO-mediated oxidation and carboxymethylation (Asad et al. 2018; Chinga-Carrasco 2011; Ding et al. 2018; Nie et al. 2018; Saeed et al. 2018). Previous studies had shown that pretreatment (such as enzymes, chemicals) could help reduce the energy consumption of cellulose fibers consumption to an amount of 1000 kWh/t from 20,000 to 30,000 kWh/t (Siró and Plackett 2010).

However, chemical pretreatment will result in a significant reduction in the mechanical strength and thermal degradation points of cellulose nanofibers (Fukuzumi et al. 2009). Compared with the high capital cost and difficult drug recycling of chemical pretreatment, enzymatic pretreatment is considered a promising process for industrial applications due to its high selectivity, low chemical loading and environmentally friendly process (Bian et al. 2018; Facundo et al. 2015; Guo et al. 2017; Kumar et al. 2016). Various studies had reported the use of mild enzymatic hydrolysis combined with refining and homogenization to produce CNF from wood pulp. It was found that the selective and mild hydrolysis using a one-component endoglucanase allowed for a larger aspect ratio and less aggregation compared to acid hydrolysis (Henriksson et al. 2007b; López-Rubio et al. 2007; Paakko et al. 2007; Siddiqui et al. 2011). Therefore, a wide range of commercial cellulases are in demand mainly composed of endoglucanases and may have great potential to promote the downstream decomposition of cellulose fibers. Although the deconstruction model of enzymatically hydrolyzed cellulose fibers has been proposed, there are few reports about systematic studies on the microstructure properties such as hydrogen bonding/cleaving and crystal structure during enzyme pretreatment.

The objective of this work was to study the microstructure and properties of BHKP cellulose fibers pretreated with commercial endoglucanases. This type of pretreatment method was chosen because of its potential to commercialize nanocellulose. A thorough investigation of the effect of pretreatment time on the microstructure and properties of cellulose fibers was conducted, including water retention value, aspect ratio, degree of polymerization, morphology, crystal structure and H-bonds pattern. This is critical for the future development of more economical pretreatment technologies and commercial promotion of nanocellulose.

2. Material And Methods

2.1 Material

The cellulose source was never-dried bleached hardwood kraft pulp (BHKP) from Shandong Sun Paper Company. Commercial endoglucanase (OEM-9) was obtained from Doing-higher (Guangxi, China). The optimum pH and temperature for the OEM-9 were 5.5 and 40°C, respectively. Enzyme activity was 8.62 IU/ml measured by the dinitrosalicylic acid (DNS) method with D-glucose as the standard.(Sengupta et al. 2000) The cupriethylenediamine hydroxide solution was provided by Tianjin Zhentai Chemical Co., Ltd. (Tianjin, China). All chemical reagents were purchased and used without further purification.

2.2 Enzymatic pretreatment

The procedure was carried out according to the previously published enzymatic pretreatment (Henriksson et al. 2007a). Briefly, 2wt% of BHKP was enzymatically hydrolyzed in citric acid-sodium citrate buffer (pH 5.5) for different times in an incubation shaker. The enzyme dosage and temperature were 10mg/g cellulose and 40°C respectively. After the hydrolysis, the slurry was centrifuged at 3000 rpm for 10 minutes to separate the solid phase and the liquid phase. The yield of cellulose was calculated by following formula: $Y = m_1/m_2*100\%$. Where Y is the yield of cellulose (%), m_1 and m_2 are the weight of cellulose before and after pretreatment, respectively.

2.3 Average molecular weight and crystal structure

The viscosity of cellulose before and after pretreatment measured by ASTM method (ASTM D1795-94, 2001) was used to calculate the degree of polymerization (DP) according to the following formula: $DP^{0.905} = 0.75[\eta]$. The crystallinity of each sample was determined by an X-ray diffractometer (XRD, D8-ADVANCE, Germany) using Cu-Ka radiation at 40 kV and 30 mA in an angular range of 10°-40° at 2.0°/min. All XRD patterns were baseline corrected from 2θ 10°-40° and single crystalline peaks and amorphous peaks were separated by Peakfit v4.12 software (Vanderfleet et al. 2018). The CrI was calculated according to the following formula: $CrI = (I_{200}-I_{am})/I_{200}*100\%$. Where I_{200} is the intensity of the (200) peak close to 22.5°, and I_{am} is the intensity at the minimum at about 18.6°. The crystallite sizes perpendicular to different lattice planes (L_{hkl}) were calculated following Scherrer formula: $L_{hkl} = 0.9\lambda / B_{hkl}\cos\theta$. Where λ is the X-ray wavelength, B_{hkl} is the angular PWHM in radians of the line profile, and θ is the scattering angle (Ling et al. 2019).

2.4 Morphological structure and size distribution

The surface morphology of samples were characterized by Scanning Electron Microscope (SEM, MERLIN Compact, Zeiss, Germany). The water retention value (WRV) was measured and calculated according to ISO 23714:2007. Average size distribution was determined by a fiber quality analyzer (FQA, LAD02, Canada).

2.5 Fourier transform infrared spectroscopy (FT-IR)

FTIR characterization was performed with a Vertex70 Hyperion FTIR spectrometer in absorbance mode using the KBr pellet technique. Spectra were acquired for a total of 32 scans in the range of 500–4000 cm^{-1} with a resolution of 4 cm^{-1}. The second derivative spectra (3700 – 3000 cm^{-1}) were calculated by the Savitzky–Golay method after the spectra were subjected to smoothing. Peakfit software (v4.12) combined with Gaussian distribution function is used to fit the spectrum in the range of 3700 – 3000 cm^{-1} to analyze the changes in H-bonds. All generalized two-dimensional correlation spectral (2DCOS) analyses were performed in 2D-shige software (Buchanan and Wei 2018).

3. Results And Discussion

3.1 Physical and chemical properties of pretreated cellulose

Enzyme pretreatment have been used to loosen the cellulose fibers to reduce energy consumption of isolation CNFs from cellulose prior to mechanical refining. It was necessary to explore the mechanism of enzyme pretreatment on the physical and chemical properties and microstructure of cellulose, which may provide theoretical support for the commercial production of CNFs. Figure 1 exhibited the effect of pretreatment time on fiber physical and chemical properties at a constant enzyme dosage of 10 mg/g, a physical temperature of 40°C and a pH of 5.5. It can be seen that the yield of cellulose gradually decreases and the water retention value gradually increases with the extension of the pretreatment time (Fig. 1a). The decrease in yield was due to the hydrolysis of cellulose by OEM-9 into soluble sugars or oligosaccharides (Kumar et al. 2016). And the more exposed hydroxyl groups can absorb more bound water to increase the WRV (Nie et al. 2018). The length and width of cellulose decreased by 78% and 21%, respectively, relative to the raw material when the pretreatment time was 10h (Fig. 1b). This tendency to decrease in the longitudinal direction resulted in a significant decrease in the aspect ratio of cellulose by 72%. It can be predicted that the pretreatment of OEM-9 will negatively affect the length of fibrils that disintegrate from the pretreated fiber. In addition, the degree of polymerization and fine components had been reduced with the prolonging of pretreatment time. It proved that OEM-9 mainly cleaved β-1, 4-glycosidic bonds of cellulose chains in the pretreatment stage and hydrolyzed into oligosaccharides (Yuan et al. 2017).

3.2 Microscopic and crystalline structure of pretreated cellulose

The surface topography of the fibers with different pretreatment times were analyzed by SEM in Fig. 2. As the pretreatment time increases, the size of the pretreated fiber gradually became smaller and the surface became wrinkled and rougher. This was consistent with the data measured by the Fiber Quality Analyzer (FQA) (Fig. 1b). In addition, significant fibrillation and breakage could be observed on the surface of pretreated fibers, which indicated that OEM-9 could facilitate the peeling of fibrils.

X-ray diffraction analysis of cellulose fiber was performed to study the effect of cellulose micro-crystal structure during the enzyme pretreatment process, as shown in Fig. 3. It could be seen that all the samples showed the cellulose-Iβ crystal structure which had a preferred orientation along the fiber axis typical of plant fibers (Fig. 3a). All XRD patterns showed obvious diffraction peaks at 15.2°, 16.5°, 22.5° and 34.5° respectively assigned to (1–10), (110), (200) and (004) reflections. It can be seen that the crystallinity index and crystallite size increase slightly with the extension of the pretreatment time (Fig. 3b). The crystallinity index and crystallite size of cellulose fiber increased by 1.7% and 5.7%, respectively, when the pretreatment time was 10h. It can be predicted that OEM-9 pretreatment only loose the amorphous area of cellulose without causing hydrolysis. This can be explained by the random cleavage of β-1,4-glycosidic bonds in the cellulose chains and cellulose fibers, resulting in the distortion of the crystallite size in the cellulose fibers (Kumar et al. 2016).

3.3 H-bonds pattern of pretreated cellulose

Figure 4 showed pretreatment-time-dependent FTIR spectra of cellulose fiber with different enzyme pretreatment time. The broad region 3700–3000cm^{-1} was assigned to –OH vibrations. The peak at 2900cm^{-1} was related to the aliphatic saturated CH_2 and CH_2OH stretching vibration of the cellulose. The absorption peak in the 1590cm^{-1} band was due to bound water and carboxylate. The characteristic peaks from 1400 to 1300cm^{-1} were attributed to the acetyl and uronic acid ester groups of cellulose. The absorption peak at 1030 cm^{-1} was assigned as the CO stretch at the C_3 position. The absorption peak at 670 – 550 cm^{-1} was related to CH deformation and OH out-of-plane bending. The hydrogen bond network structure inside cellulose is mainly composed of intramolecular and intermolecular hydrogen bonds (3700–3000cm^{-1}). It can be see that the absorbance of the 3000-3700cm^{-1} region generated by the stretching vibration of the intermolecular and intramolecular H-bonds increased with the elapse of pretreatment time. According to previous reports, the band assignments for O-H stretching region in cellulose can be observed through the second derivative spectra (Watanabe et al. 2006). The second derivative spectra (3700-3000cm^{-1}) of cellulose with different enzyme pretreatment time as shown in Fig. 4 (b). There are three distinct peaks that can be identified in this region. These three peaks are assigned to the OH stretching modes of cellulose.

To explore the effect of pretreatment on the H-bonds of cellulose fibers, FTIR in the range of 3700-3000cm^{-1} was used to evaluate the content of different types of H-bonds. This region can be divided into intermolecular H-bonds for O6H6···O3' and intramolecular H-bonds for O3H3···O5 and O2H2···O6 *via* PeakFit (v4.12) as shown Fig. 5 (a-f)(Wan et al. 2015). The contents and peak positions of the three H-bond models were shown in Table 1 and Fig. 5 (g). The content of O6H6···O3' (intermolecular H-bonds) decreased from 69% (raw cellulose) to 53% ($Time_{10}$) with the extension of the pretreatment time. And the peak position of O6H6···O3' shift to a higher wavelength as the pretreatment time elapses. The significantly larger wavenumber shift is probably due to the disruption of the H-bonds between the OH groups of the cellulose molecular chain.(Watanabe et al. 2006) The content and peak position of intramolecular H-bonds (O3H3···O5 and O2H2···O6) did not change significantly with the extension of the pretreatment time. This ambiguous shift indicated that the OEM-9 did not directly affect the intramolecular H-bonds and the interaction was very complicated (Laine and E. 1982). This result indicated that OEM-9 interact more easily with the O6H6···O3' rather than O3H3···O5 and O2H2···O6. This may be beneficial to improve the aspect ratio and tensile strength of the fibrils separated from the pretreated fiber.

Table 1
Evolution of different hydrogen bond content with pretreatment time.

Time (h)	Wavenumber (cm^{-1})	H-bonds	Content (%)	R^2
0	3286.3	O6H6···O3'	0.69	0.9934
	3483.2	O3H3···O5	0.24	
	3582.9	O2H2···O6	0.07	
2	3294.9	O6H6···O3'	0.67	0.9934
	3493.1	O3H3···O5	0.26	
	3590.8	O2H2···O6	0.07	
4	3300.2	O6H6···O3'	0.64	0.9950
	3497.7	O3H3···O5	0.27	
	3593.1	O2H2···O6	0.09	
6	3302.9	O6H6···O3'	0.63	0.9976
	3502.2	O3H3···O5	0.28	
	3597.4	O2H2···O6	0.09	
8	3303.9	O6H6···O3'	0.63	0.9954
	3485	O3H3···O5	0.28	
	3582.6	O2H2···O6	0.09	
10	3317.2	O6H6···O3'	0.58	0.9971
	3492.7	O3H3···O5	0.32	
	3587.3	O2H2···O6	0.10	

To further study the sequence of OEM-9 acting on the H-bonds inside the fiber during the pretreatment process, 2DCOS was used to analyze this region (3000-3700cm^{-1}). 2DCOS can directly extend the spectral signal to two dimensions to improve the spectral resolution and reveal the sequence of changes between groups (Noda 2016a; Noda 2016b). Figure 6 showed two-dimensional synchronous correlation spectrum generated from the pretreatment-time-dependent FTIR spectra variations in the time ranges 0-10h. Figure 6 (c) depicted the corresponding auto correlation spectra extracted from the synchronized 3D and 2D correlation spectra shown in Fig. 6 (a, b). It can be seen that a strong auto peak of Φ (3400, 3400) > 0 and two shoulders of Φ (3300, 3300) > 0 and Φ (3560, 3560) > 0, which means that the three bands near 3300, 3400 and 3560 cm^{-1} all decrease with the increase of pretreatment time. The positions of the auto peaks near 3300, 3400 and 3560 cm^{-1} almost completely correspond to the peak positions fitted via PeakFit, which are assigned to the interchain H-bonds (O6H6···O3') and intramolecular H-bonds (O3H3···O5 and O2H2···O6), respectively. These results indicate that the destruction of interchain and

intrachain H-bonds in cellulose occurred during the pretreatment process. No obvious crosspeaks are observed, indicating that there is no intermolecular interaction between the three H-bond models. In other words, the process of OEM-9 cleave these three H-bonds is independent in the pretreatment process.

Figure 7 showed two-dimensional asynchronous correlation spectrum generated from the pretreatment-time-dependent FTIR spectra variations in the time ranges 0-10h. The slice spectra extracted from the asynchronous 3D and 2D correlation spectra (Fig. 7a, b) at 3497cm-1 was depicted in Fig. 7(c). It can be seen that the slice spectra at 3497 cm^{-1} had asynchronicity with the peaks appearing at 3350 and 3600 cm^{-1}. The slice position at 3497 cm^{-1} corresponds to the intramolecular H-bonds (O3H3···O5) in cellulose (Wan et al. 2015). The negative peak at Ψ (3497, 3350) < 0 and positive peak at Ψ (3497, 3600) > 0 were attributed to interchain H-bonds (O6H6···O3') and intramolecular H-bonds (O2H2···O6), respectively. According to the fundamental rules of asynchronous spectroscopy, the spectral intensity change at 3497 cm^{-1} occurs before that at 3350 cm^{-1} and behind that at 3600 cm^{-1}. It can be concluded that the sequence of changes in the H-bonds structure of cellulose during enzymatic hydrolysis is interchain H-bonds (O6H6···O3') > intramolecular H-bonds (O3H3···O5) > intramolecular H-bonds (O2H2···O6).

4. Conclusions

In conclusion, this study investigated the dynamic evolution of properties and microstructure of enzyme pretreated cellulose. We concluded that properties and microstructure of cellulose could be controlled dramatically by the pretreatment time, such as yield, water retention value, aspect ratio, degree of polymerization, crystallinity and H-bonds. The intermolecular H-bonds with the most significant decrease in content (16%) was cleaved first relative to the intramolecular H-bonds. This unique study is of great value for the commercial production of fibrils through enzymatic hydrolysis.

Declarations

Acknowledgements

The Project Supported by the Foundation (No. ZZ20200107) of State Key Laboratory of Biobased Material and Green Papermaking, Qilu University of Technology, Shandong Academy of Sciences and Guangdong Basic and Applied Basic Research Foundation (2019A1515110708).

Funding

This study has no financial interest.

Conflicts of interest/Competing interests

The authors declare that they have no conflict of interest.

Ethical approval

This article does not contain any studies with human participants or animals performed by any of the authors.

Authors' contributions

All authors contributed as the main contributors of this work. Ronggang Li and Qijun Ding had the idea for the article. All authors performed the literature search and analysis. All authors had drafted, revised the work and approved the final paper.

References

1. Asad M, Saba N, Asiri AM, Jawaid M, Indarti E, Wanrosli WD (2018) Preparation and Characterization of Nanocomposite Films from Oil Palm Pulp Nanocellulose/Poly (Vinyl alcohol) by Casting Method Carbohydrate Polymers 191,103–111
2. Bian H, Gao Y, Yang Y, Fang G, Dai H (2018) Improving cellulose nanofibrillation of waste wheat straw using the combined methods of prewashing, p -toluenesulfonic acid hydrolysis, disk grinding, and endoglucanase post-treatment Bioresource Technology:321–327
3. Buchanan LE, Wei X (2018) Two-Dimensional Infrared (2D IR) Spectroscopy Encyclopedia of Modern Optics:164–183
4. Chinga-Carrasco G (2011) Cellulose fibres, nanofibrils and microfibrils: The morphological sequence of MFC components from a plant physiology and fibre technology point of view. Nanoscale Res Lett 6(1):417–424
5. Daud SM, Kim BH, Ghasemi M, Wan RWD (2015) Separators used in microbial electrochemical technologies: Current status and future prospects. Biores Technol 195:170–179
6. Ding Q, Zeng J, Wang B, Tang D, Chen K, Gao W (2018) Effect of Nanocellulose Fiber Hornification on Water Fraction Characteristics and Hydroxyl Accessibility during. Dehydration Carbohydrate Polymers 207:44–51
7. Dufresne A (2017) Cellulose nanomaterial reinforced polymer nanocomposites. Current Opinion in Colloid Interface ence 29:1–8
8. Facundo et al (2015) Increasing yield of nanocrystalline cellulose preparation process by a cellulase pretreatment. Biores Technol 192:574–581
9. Fukuzumi H, Saito T, Iwata T, Kumamoto Y, Isogai A (2009) Transparent and High Gas Barrier Films of Cellulose Nanofibers Prepared by TEMPO-Mediated. Oxidation Macromolecules *Macromolecules* 10:162–165
10. Guo H, Chang Y, Lee DJ (2017) Enzymatic saccharification of lignocellulosic biorefinery. Research focuses Bioresource Technology 252:198–215
11. Henriksson M, Henriksson G, Berglund LA, Lindström T (2007a) An environmentally friendly method for enzyme-assisted preparation of microfibrillated cellulose (MFC) nanofibers. Eur Polymer J 43:3434–3441

12. Henriksson M, Henriksson G, Berglund LA, Lindstr?M T (2007b) An environmentally friendly method for enzyme-assisted preparation of microfibrillated cellulose (MFC) nanofibers. Eur Polymer J 43:3434–3441
13. Jonoobi M, Oladi R, Davoudpour Y, Oksman K, Dufresne A, Hamzeh Y, Davoodi R (2015) Different preparation methods and properties of nanostructured cellulose from various natural resources and residues:. a review Cellulose 22:935–969
14. Kumar M, Singhal A, Thakur IS (2016) Comparison of submerged and solid state pretreatment of sugarcane bagasse by Pandoraea sp. ISTKB: Enzymatic structural analysis Bioresource Technology 203:18–25
15. López-Rubio A, Lagaron JM, Ankerfors M, Lindstr?M T, Nordqvist D, Mattozzi A, Hedenqvist MS (2007) Enhanced film forming and film properties of amylopectin using micro-fibrillated. cellulose Carbohydrate Polymers 68:718–727
16. Laine HS, E. J (1982) Modification of Lignins. I. Reaction of Lignins with Chlorophosphazenes. Journal of Macromolecular Science: Part A - Chemistry 17(8):1193–1202
17. Lavoine N, Desloges I, Dufresne A, Bras J (2012) Microfibrillated cellulose – Its barrier properties and applications in cellulosic materials. A review Carbohydrate Polymers 90:735–764
18. Ling Z et al (2019) Effects of ball milling on the structure of cotton cellulose Cellulose 26, 305–328
19. Nechyporchuk O, Belgacem MN, Bras J (2016) Production of cellulose nanofibrils: A review of recent advances Industrial. Crops Products 93:2–25
20. Nie S, Zhang K, Lin X, Zhang C, Yan D, Liang H, Wang S (2018) Enzymatic pretreatment for the improvement of dispersion and film properties of cellulose. nanofibrils Carbohydrate Polymers 181:1136–1142
21. Noda I (2016a) Generalized Two-Dimensional Correlation Method Applicable to Infrared, Raman, and other Types of. Spectroscopy Applied Spectroscopy 47:1329–1336
22. Noda I (2016b) Two-Dimensional Infrared (2D IR) Spectroscopy: Theory. and Applications Applied Spectroscopy 44(4):550–561
23. Paakko et al (2007) Enzymatic hydrolysis combined with mechanical shearing and high-pressure homogenization for nanoscale cellulose fibrils and strong gels BIOMACROMOLECULES 2007,8(6):1934–1941
24. Saeed HAM, Liu Y, Lucia LA, Chen HL (2018) Sudanese Dicots as Alternative Fiber Sources for Pulp and Papermaking *Drvna Industrija*, 69, 175–182
25. Sengupta S, Jana ML, Sengupta D, Naskar AK (2000) A note on the estimation of microbial glycosidase activities by dinitrosalicylic acid reagent. Applied Microbiology Biotechnology 53:732–735
26. Siddiqui N, Mills RH, Gardner DJ, Bousfield D (2011) Production and Characterization of Cellulose Nanofibers from Wood Pulp. Journal of Adhesion ence Technology 25:709–721

27. Siró I, Plackett D (2010) Microfibrillated cellulose and new nanocomposite materials:. a review Cellulose 17:459–494
28. Vanderfleet OM, Reid MS, Bras J, Heux L, Godoy-Vargas J, Panga MKR, Cranston ED (2018) Insight into thermal stability of cellulose nanocrystals from new hydrolysis methods with acid blends Cellulose 26, 507–528
29. Wan J, Lian J, Wang Y, Ma Y (2015) Investigation of cellulose supramolecular structure changes duringconversion of waste paper in near-critical water on producing5-hydroxymethyl furfural -. ScienceDirect Renewable Energy 80:132–139
30. Watanabe A, Morita S, Kokot S, Matsubara M, Fukai K, Ozaki Y (2006) Drying process of microcrystalline cellulose studied by attenuated total reflection IR spectroscopy with two-dimensional correlation spectroscopy and principal component analysis. J Mol Struct 799:102–110
31. Yuan C, Yuchan H, Dongbin F, Yanming H, Gaiyun L, Siqun W (2017) An Efficient Method for Cellulose Nanofibrils Length Shearing via Environmentally Friendly Mixed Cellulase Pretreatment Journal of Nanomaterials,2017,(2017-3-23) 2017:1–12
32. Zhu H et al (2016) Wood-Derived Materials for Green Electronics, Biological Devices, and Energy Applications Chemical Reviews 116:9305–9374

Figures

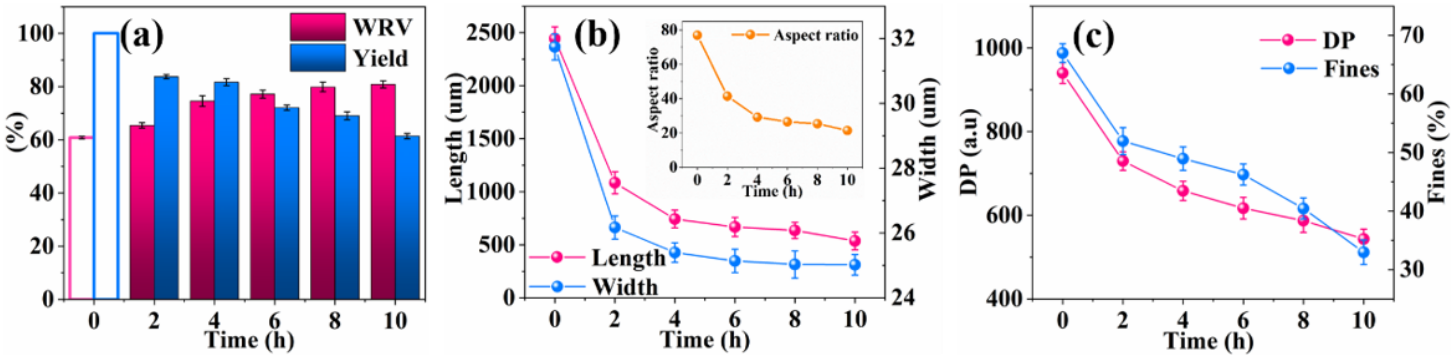

Figure 1

The effect of enzyme pretreatment time on the physical and chemical properties of cellulose fiber. (a) Yield rate and water retention value (WRV). (b) Length and width. Inset: aspect ratio. (c) Degree of polymerization (DP) and fines.

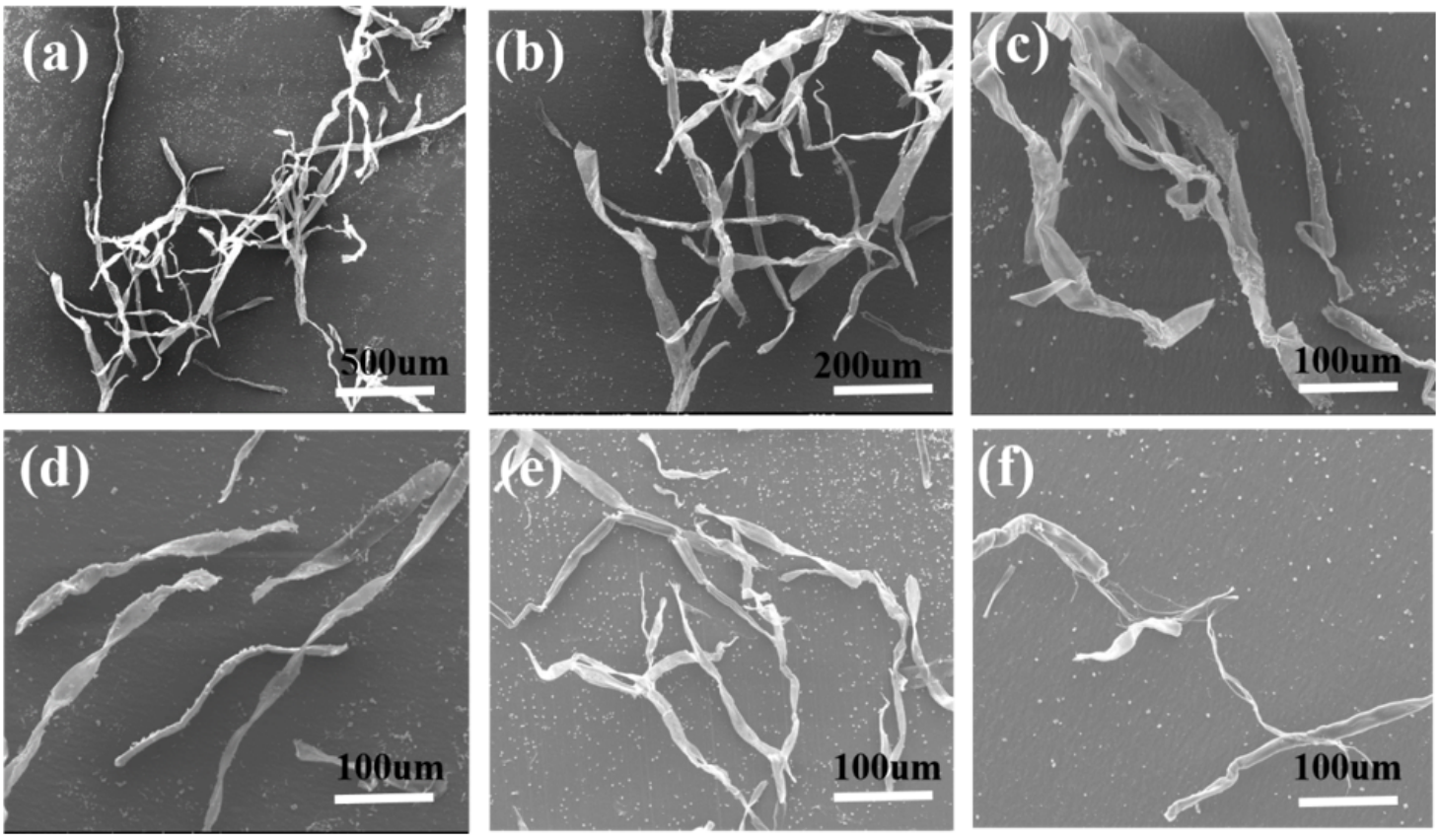

Figure 2

SEM images of cellulose fiber with different pretreatment time. (a) 0h, (b) 2h, (c) 4h, (d) 6h, (e) 8h and (f) 10h.

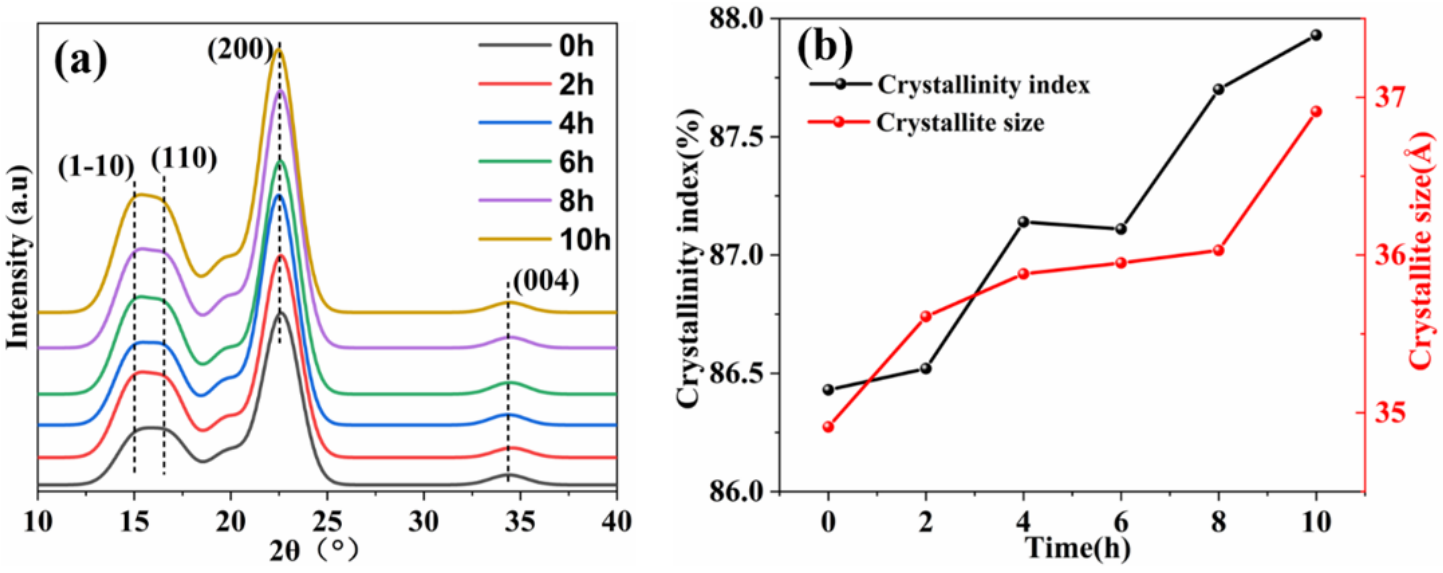

Figure 3

XRD patterns (a), crystallinity index and crystallite size (b) of cellulose with different enzyme pretreatment time.

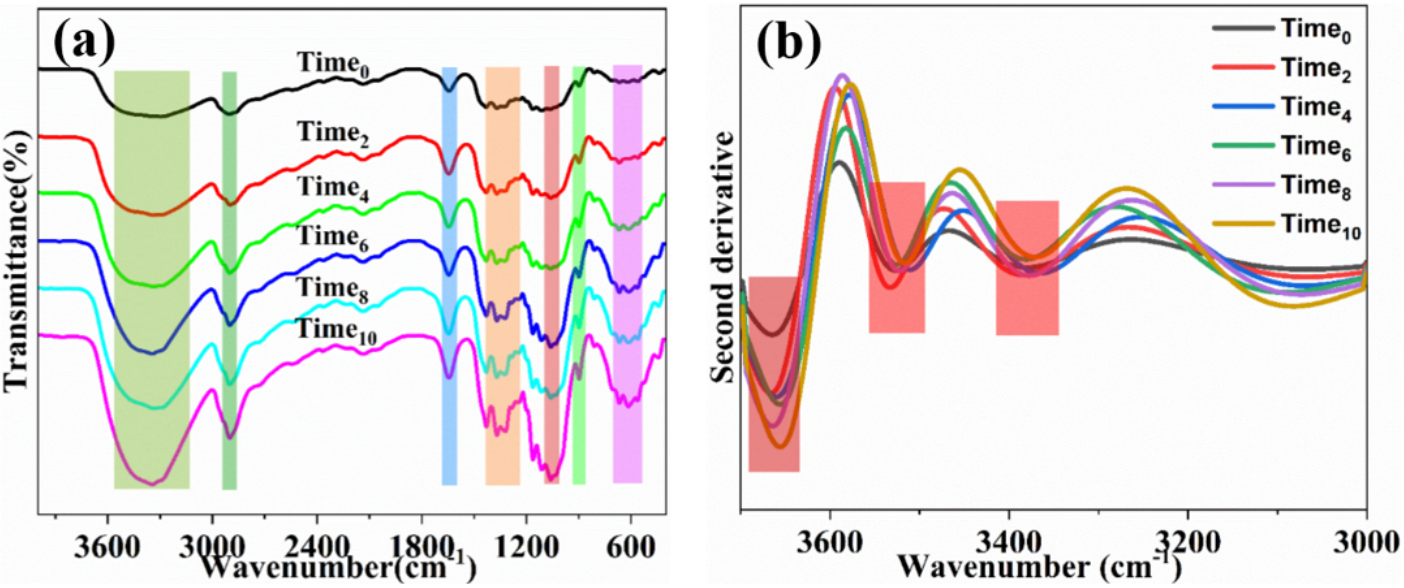

Figure 4

Pretreatment-time-dependent FTIR spectra and second derivative spectra (3700-3000cm-1) of cellulose with different enzyme pretreatment time.

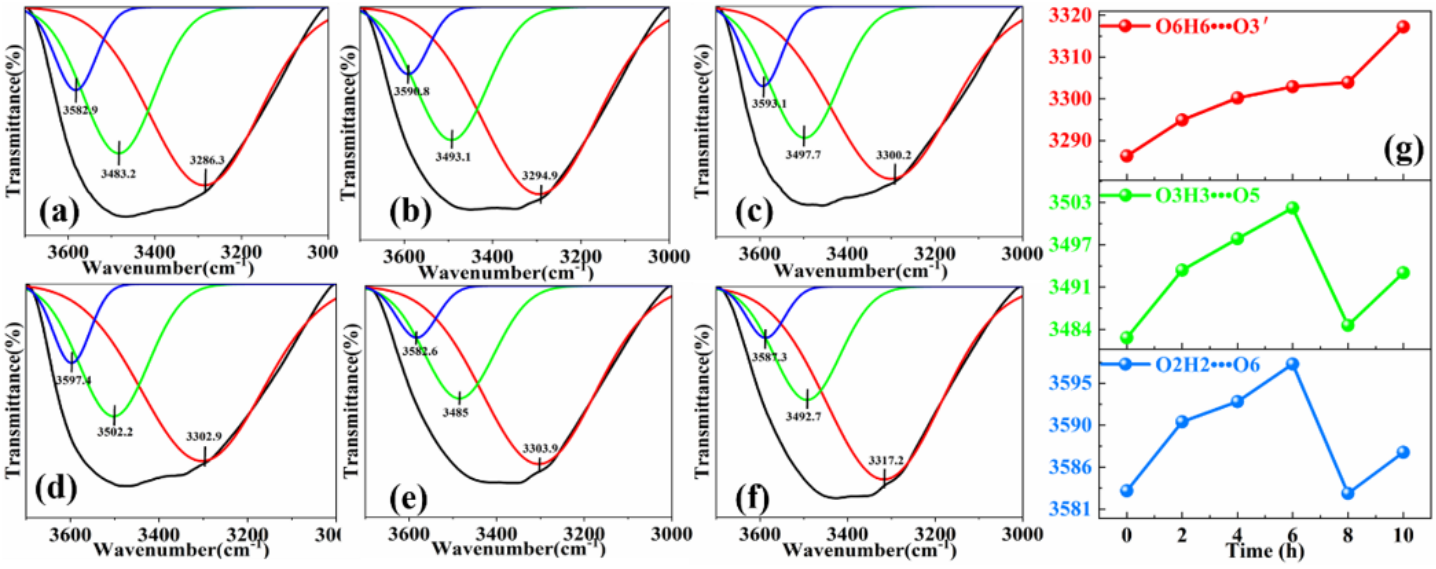

Figure 5

(a - f) Different H-bond models obtained from FTIR peak fitting via PeakFit in the 3700-3000cm-1. (g) Peak positions of different H-bond models as a function of the pretreatment time.

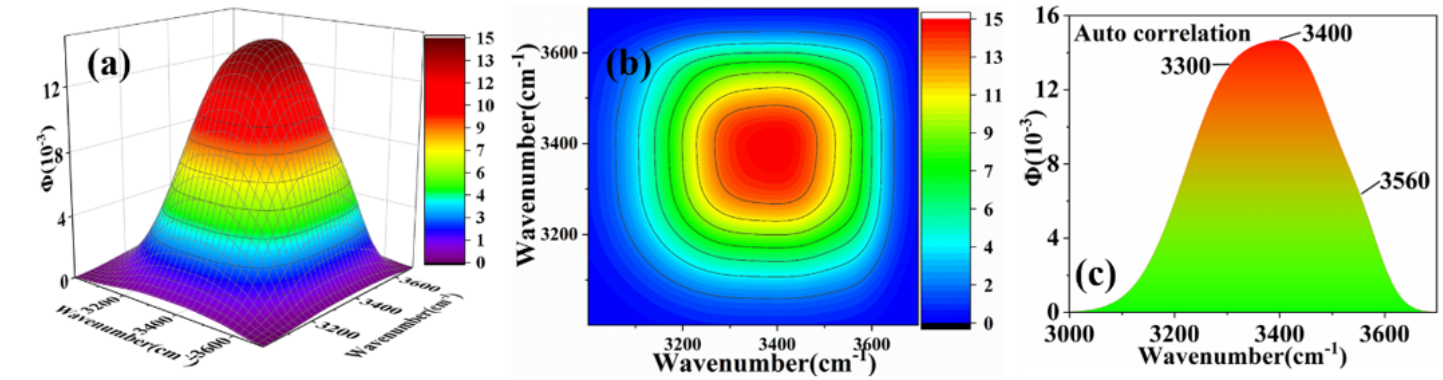

Figure 6

Two-dimensional synchronous correlation spectrum of pretreated cellulose (0-10h). (a) 3D synchronous map. (b) Synchronous 2D correlation spectra. (c) Auto correlation spectra.

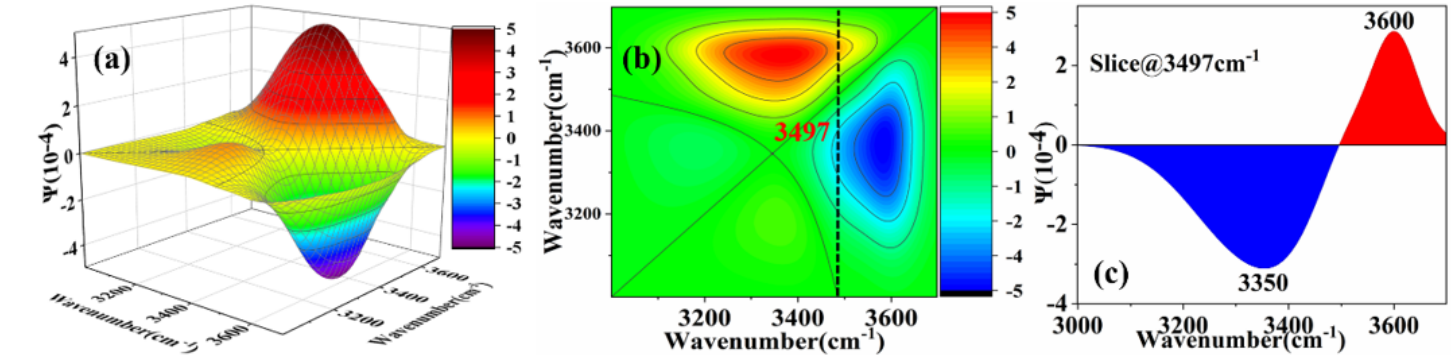

Figure 7

Two-dimensional asynchronous correlation spectrum of pretreated cellulose (0-10h). (a) 3D asynchronous map. (b) Asynchronous 2D correlation spectra. (c) Horizontal slice spectra extracted at 3497 cm-1.

Supplementary Files

This is a list of supplementary files associated with this preprint. Click to download.

- Graphicabstract.docx